Article ID: 1006-8775(2017) 03-0292-10

COMPARATIVE ANALYSIS OF VARIOUS DATA OF AIR–SEA TEMPERATURE DIFFERENCE AND ITS VARIATION ACROSS SOUTH CHINA SEA IN THE PAST 35 YEARS

XU Feng (徐 峰)[1], XIA Tian-zhu (夏天竹)[2], WANG Hui (王 慧)[3], LIU Ke-xiu (刘克修)[3]
(1. College of Oceanography and Meteorology, Guangdong Ocean University, Zhanjiang 524088 China;
2. Tianjin Binhai New Area Meteorological Bureau, Tianjin 300457 China;
3. National Marine Data & Information Service, Tianjin 300171 China)

Abstract: Using the International Comprehensive Ocean-Atmosphere Data Set (ICOADS) and ERA-Interim data, spatial distributions of air-sea temperature difference (ASTD) in the South China Sea (SCS) for the past 35 years are compared, and variations of spatial and temporal distributions of ASTD in this region are addressed using empirical orthogonal function decomposition and wavelet analysis methods. The results indicate that both ICOADS and ERA-Interim data can reflect actual distribution characteristics of ASTD in the SCS, but values of ASTD from the ERA-Interim data are smaller than those of the ICOADS data in the same region. In addition, the ASTD characteristics from the ERA-Interim data are not obvious inshore. A seesaw-type, north-south distribution of ASTD is dominant in the SCS; i.e., a positive peak in the south is associated with a negative peak in the north in November, and a negative peak in the south is accompanied by a positive peak in the north during April and May. Interannual ASTD variations in summer or autumn are decreasing. There is a seesaw-type distribution of ASTD between Beibu Bay and most of the SCS in summer, and the center of large values is in the Nansha Islands area in autumn. The ASTD in the SCS has a strong quasi-3a oscillation period in all seasons, and a quasi-11a period in winter and spring. The ASTD is positively correlated with the Niño3.4 index in summer and autumn but negatively correlated in spring and winter.

Key words: marine meteorology; air-sea temperature difference; comparison of data; empirical orthogonal function decomposition; wavelet analysis; ERA-Interim
CLC number: P732 **Document code:** A
doi: 10.16555/j.1006-8775.2017.03.006

1 INTRODUCTION

For hundreds of years, under the background of climate warming, global air temperature and sea surface temperature (SST) have gradually increased, with the air-sea temperature difference (ASTD) constantly changing. The ASTD is an important parameter in the study of exchange at the air–sea interface, which has a great impact on the variation of sea fog, land-sea breezes and even wind stress in coastal areas.

Sea fog is a weather phenomenon in which the condensation of water vapor generates a large number of droplets, causing visibility less than 1,000 m under oceanic influence (Wang[1]). Because the oceanic impact on the atmosphere is mainly manifested in change of temperature and humidity in the boundary layer, the ASTD is an important topic in the study of the mechanism of sea fog. The study of Zhang et al. [2] showed that air temperature drops substantially when spring sea fog occurs over the Huanghai Sea, and the ASTD (T minus SST) decreases to < 0.5℃. When the sea fog dissipates, the ASTD increases remarkably, and when thick fog occurs, SST is even warmer than air temperature. Research into the boundary layer structure of sea fog over coastal regions of South China (Huang et al.[3]) also indicates that during sea fog episodes, the ASTD shows that air temperature of the near sea-surface is mostly warmer than SST at the Bohe station, Maoming, Guangdong.

The variations of ASTD are closely related to the formation of the sea–land breeze. Yang et al. [4] pointed out that in the first half of the year (January–May), ASTD decreases and the atmospheric stratification is stable. It thus is difficult for the sea-land breeze to form and develop the thermodynamic circulation. In the second half of the year (September–December), the ASTD increases and the atmospheric stratification is instable. This is advantageous for the sea–land breeze to form and develop the thermodynamic circulation. Moreover, Lin et al.[5] stated that during winter over the Indian Ocean and spring over the equatorial central Pacific Ocean, as well as summer over the South China Sea (SCS) and Western Pacific, the ASTD is strongly

Received 2016-03-21; **Revised** 2017-07-10; **Accepted** 2017-08-15
Foundation item: National Natural Science Foundation of China (41475120)
Biography: XU Feng, Ph. D., professor, primarily undertaking research on atmospheric physics and marine meteorology.
Corresponding author: XIA Tian-zhu, e-mail: helenxtz2012@163.com

associated with summer monsoon convection over the SCS.

The ASTD is also used in research of sea surface wind stress. This stress is the major driver of upper-layer oceanic circulations and ocean waves, reflecting the transport of turbulent momentum at the air-sea interface. Thus, accurately estimating wind stress at the sea surface is essential for air-sea interaction to simulate and predict the dynamic process. In previous studies, it was widely believed that wind stress (drag coefficient C_D) only depends on sea surface wind speed, with a linear relationship. Ji et al.[6] gave a corrected formula for the ASTD drag coefficient. They did not believe that wind stress is related only to wind speed but that it is also affected by the ASTD.

The variations of ASTD are also related to season, region, and other factors. Xue et al.[7] stated that the Qingdao seashore ASTD is larger in autumn and winter, smaller in spring and summer, with a maximum value in December and minimum in March. Wang et al.[8] indicated that the ASTD has seasonal variations on the north and south sides of the Shandong Peninsula; northerly winds prevail in autumn and winter, which make the oceanic influence on the north side greater than on the south side. Thus, the absolute value of ASTD on the north side (Yantai) is less than the south side (Qingdao). However, southerly winds prevail in spring and summer, which makes the oceanic influence on the north side less than on the south side. Therefore, the absolute value of ASTD on the north side is greater than on the south side.

In summary, in various fields, scholars have extensively researched the ASTD in many aspects. However, this research has mainly focused on the effect of certain atmospheric or oceanic processes on ASTD. There has been less fundamental study of ASTD temporal and spatial distributions in specific sea areas. In the present article, European Center for Medium-Range Weather Forecasts (ECMWF) reanalysis data (ERA-Interim) and the International Comprehensive Ocean–Atmosphere Data Set (ICOADS) are used, comparing and analyzing the distributions of ASTD with various data of the SCS. In addition, the spatiotemporal characteristics of ASTD in this area are discussed.

2 DATA AND METHODS

2.1 *Data*

(1) The ECMWF ERA-Interim reanalysis provides worldwide gridded data. Monthly mean SST and air temperature at 2 meters above sea level were used. The period is March 1979 through February 2014, and spatial resolution is 0.125° × 0.125°.

(2) National Climatic Data Center furnishes ICOADS, which is also worldwide gridded data. Monthly mean SST and air temperature were used. The period is again March 1979 through February 2014, and spatial resolution is 1° × 1°.

(3) For NCEP Climate Prediction Center data of the Niño3.4 index (East-central Pacific SST), the period was March 1979 through February 2014 and the region was 170°–120°W, 5°N–5°S .

2.2 *Definition of ASTD*

Because scholars from different fields calculate ASTD using different equations, for comparative purposes, we defined it using

$$\triangle T=T-T_S \tag{1}$$

where $\triangle T$ stands for ASTD (℃), T for sea-surface air temperature (℃), and T_S for SST (℃).

2.3 *Data processing methods*

Based on empirical orthogonal function (EOF) decomposition, intra-annual and interannual changes of ASTD across the SCS were analyzed by their spatial distribution and temporal variation. This was done as follows.

According to the intra-annual and interannual change, monthly mean data of ASTD were converted to anomalies, given in the form of the matrix

$$X=\begin{bmatrix} x_{11} & \cdots & x_{1j} & \cdots & x_{1n} \\ \vdots & \vdots & \vdots & \vdots & \vdots \\ x_{i1} & \cdots & x_{ij} & \cdots & x_{in} \\ \vdots & \vdots & \vdots & \vdots & \vdots \\ x_{m1} & \cdots & x_{mj} & \cdots & x_{mn} \end{bmatrix} \tag{2}$$

where m is length of time, n is the total number of grids, and x_{ij} indicates the ASTD anomaly at grid j at time i.

The field series (2) of ASTD was decomposed into the sum of orthogonal time functions and orthogonal space functions, that is,

$$\hat{X}=\sum_{k=1}^{H} t_{hi}l_{hj} \qquad \begin{matrix} i=1,2,\cdots,m \\ j=1,2,\cdots,n \end{matrix} \tag{3}$$

where t_{hi} is the weight coefficient of number h characteristic field at i, which only changes with time. l_{hj} is the value of h at j, which only changes in space.

In general, the spatial function l_{hj} is regarded as a typical field, and the temporal function t_{hi} as the time weight coefficients of a typical field. Therefore, Equation (3) showing the observed ASTD field at various times is linearly superposed by a series of typical fields according to different time weight coefficients. The difference between fields just depends on time weight coefficients of different typical fields.

3 COMPARISON OF ASTD FROM TWO DATASETS

Using the ICOADS and ERA-Interim data, we calculated the spatial distribution of ASTD and its variation with season and month over the SCS for the past 35 years.

3.1 *Spatial distribution*

Using the ICOADS and ERA-Interim data, the climatic field of ASTD was calculated over the SCS for the past 35 years, as shown in Fig. 1. The results show that ASTD was negative in the central part with small

temperature difference, with large temperature differences in southern and northern parts. Based on the ICOADS data, the ASTD field nearshore shows a layered structure with small values, especially near Taiwan Island (Fig.1a). However, based on the ERA-Interim data, the ASTD field has a uniform region with small values over the entire northern SCS, from the west around Beibu Bay to the east around Taiwan (Fig.1b).

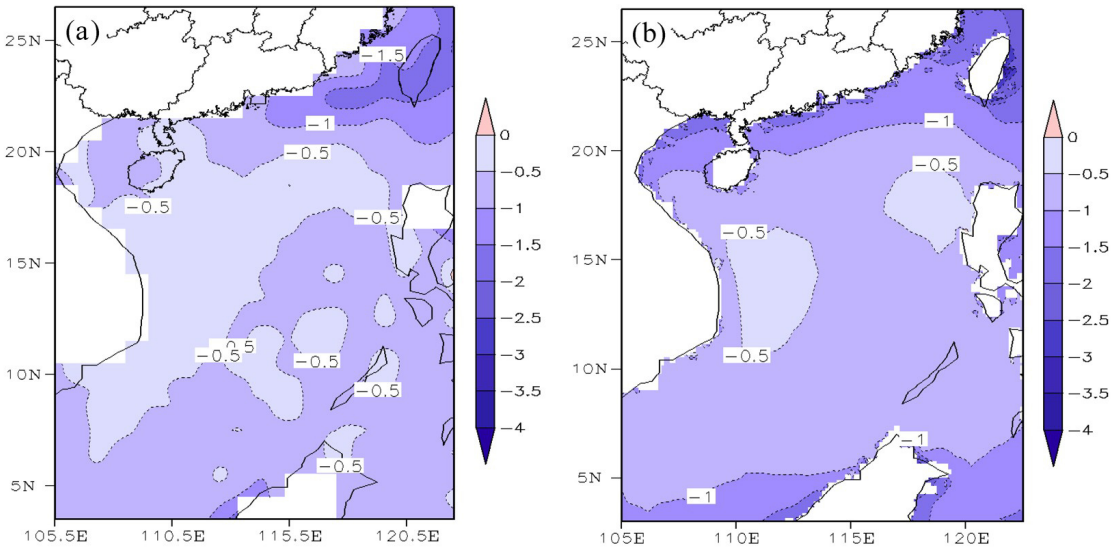

Figure 1. Average climate state of ASTD field across SCS. a. ICOADS; b. ERA-Interim.

3.2 *Seasonal variation*

The distribution of ASTD over the SCS for the past 35 years in summer (June–August) (Fig.2) shows that both datasets can reflect the major distribution characteristics. A negative ASTD area extends from south to north by numerical propulsion. There is a positive area of ASTD in the northern coastal area. In addition, the northeast part of the Indochina Peninsula extends to the waters of Beibu Bay and coastline of Guangdong Province. The positive area is more obvious from the ICOADS data (Fig.2a). However, only around the Taiwan Strait area is there a clear positive area from the ERA-Interim data, with no corresponding positive area in other northern coastal areas of the SCS (Fig.2b).

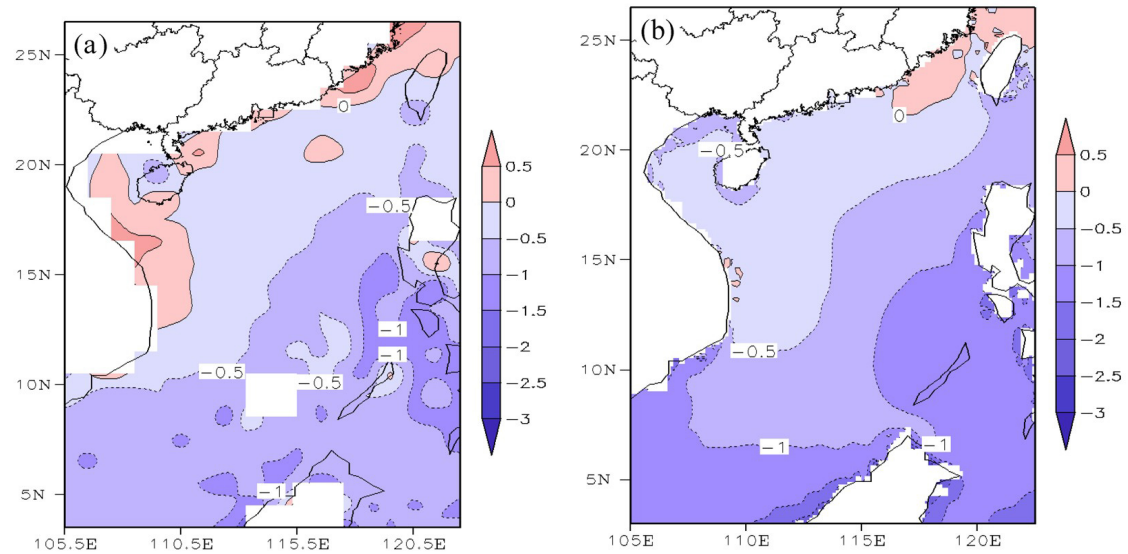

Figure 2. ASTD field over SCS in summer. a. ICOADS; b. ERA-Interim.

Figure 3 shows the ASTD field across the SCS for the past 35 years in winter (December–February). The ASTD is mainly negative and has small temperature differences in the middle SCS, and large differences on the two sides. In the northern waters of the SCS, ASTD shows a clear layered structure using both datasets. ASTD regional characteristics in the northern coastal waters are obvious from the ICOADS data. The negative ASTD area is closed in the waters of Beibu Bay, and the negative center near Taiwan extends from coastal regions to the southeast to those of South China (Fig.3a). However, using the ERA-Interim data, the negative area has a fully banded structure, with its west end in Beibu Bay to east of Taiwan (Fig.3b).

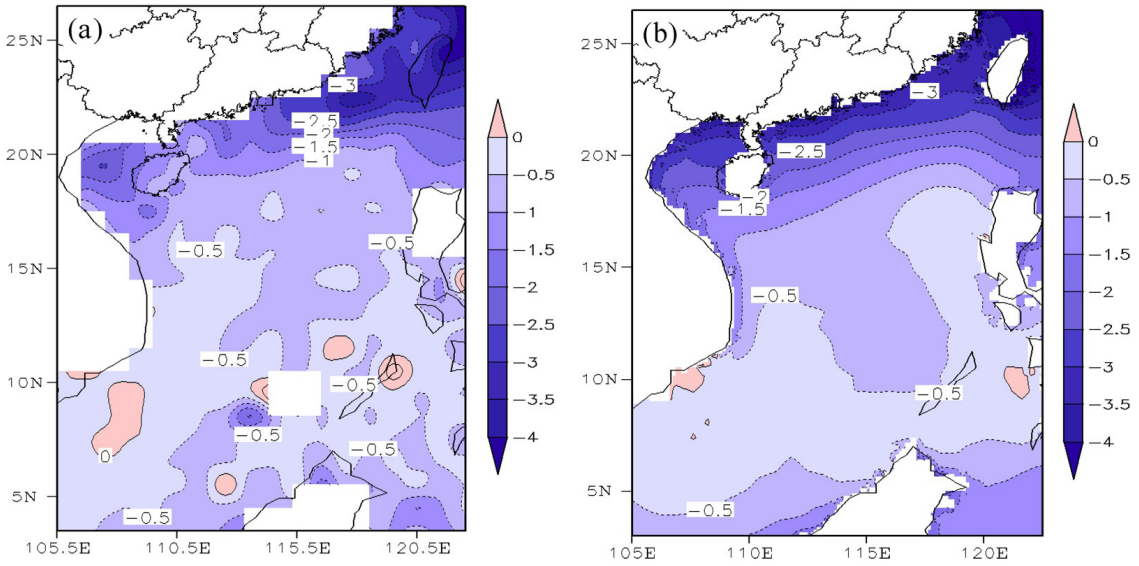

Figure 3. ASTD field over SCS in winter. a. ICOADS; b. ERA-Interim.

3.3 *Monthly analysis*

We compared the monthly ASTD field from the two datasets. We took April as an example (Fig.4). From the two datasets for spring and summer, the entire ASTD field over the SCS had a similar characteristic. Regional characteristics of the ICOADS data are more pronounced than those of the ERA-Interim data.

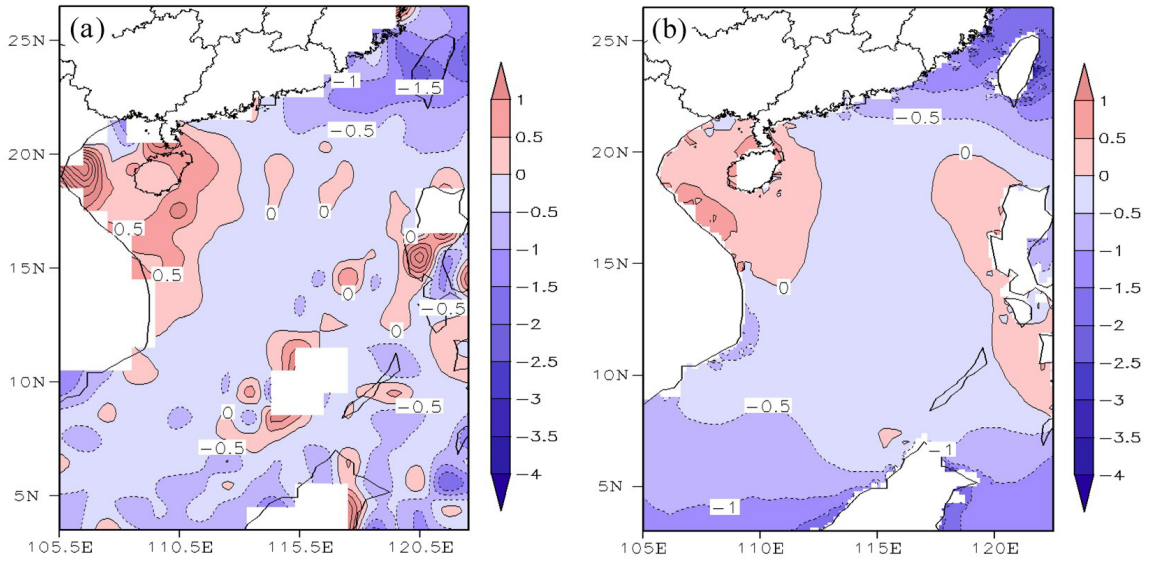

Figure 4. ASTD field over SCS in April. a. ICOADS; b. ERA-Interim.

In October, for example (Fig.5), using the ICOADS data and the ERA-Interim data, the ASTD field difference between them in autumn and winter is not substantial. Only in the nearshore area, regional characteristics of the ICOADS data are more pronounced than those of the ERA-Interim data.

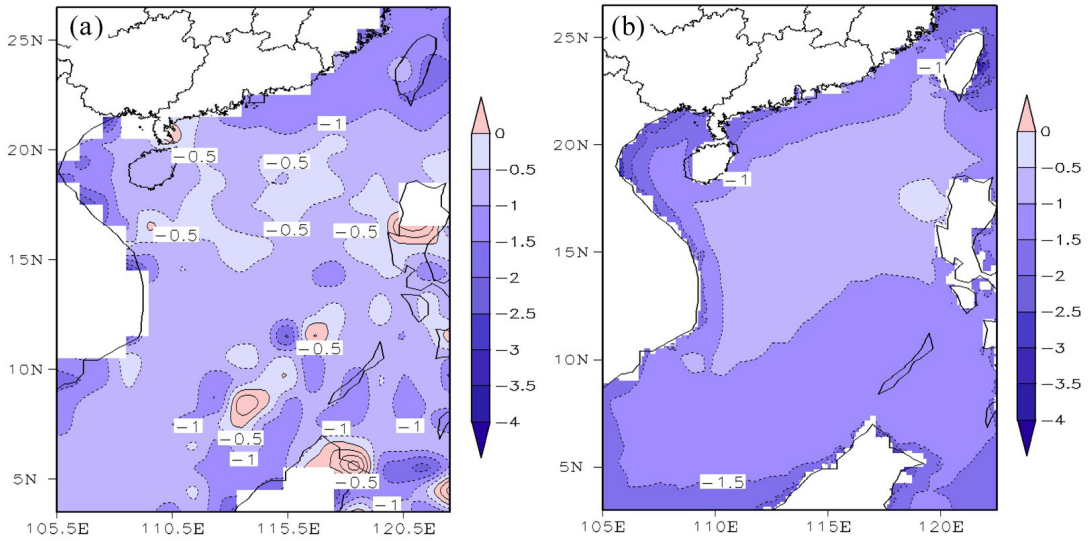

Figure 5. ASTD field over SCS in October. a. ICOADS; b. ERA-Interim.

In conclusion, using both ICOADS and ERA-Interim data, the entire ASTD field was similar across the SCS for the past 35 years. Thus, both datasets can be used to reflect the overall ASTD distribution there. However, in the same region, ASTD values from ERA-Interim data were smaller than from ICOADS data. Moreover, in describing ASTD characteristics in a specific coastal area, regional characteristics from ICOADS data are more pronounced than those from ERA-Interim data. This is because ICOADS is an ocean surface dataset formed from many countries' datasets by processing and combination. These data contain more than 2×10^8 original observation records since 1784, including measurement or observation data from vessels (commercial, naval, and research), mooring buoys and floating buoy data, coastal site data, and other ocean station data (Li et al.[9]). The data are closer to the actual field distribution in the ocean. The ERA-Interim data are from numerical models, based on assimilation data. During assimilation and numerical model operation, strong regional characteristics can be preserved while weak ones are filtered out.

4 ANALYSIS OF ASTD VARIATION

4.1 *Intra–annual variations*

It is difficult to deal with numerous missing ICOADS data, so in this section, we focus on the spatial and temporal distribution of ASTD across the entire SCS. Therefore, based on the ERA-Interim data, the monthly average ASTD anomaly in the SCS was analyzed by EOF decomposition for the past 35 years. Then, we obtained spatial and temporal distributions of intra-annual ASTD variation over the SCS. The first three rate of variance contributions of the eigenvectors were 35.88%, 22.07% and 12.40%, constituting a total of 70.35% of the information of intra-annual ASTD variation over the SCS. Combining the first mode of the eigenvectors with the time weight coefficient (Fig.6), we observed a seesaw-type ASTD distribution between the southern and northern SCS. In autumn and winter, there were negative values of ASTD in the northern SCS and positive ones in the southern SCS. In November, there was a negative peak in the north and positive peak in the south. In spring and summer, there were positive ASTD values in the northern SCS and negative ones in the south. In April and May, there was a negative peak in the south and a positive peak in the north.

Figure 7 shows the second mode of intra-annual ASTD variations across the SCS, combined with eigenvectors of the second mode and time weight coefficient. As seen, the ASTD near Taiwan Island and over most of the SCS was of the seesaw type. In winter, there were negative ASTD values near Taiwan Island and positive ones over most of the SCS. There was maximum variation of the seesaw type in January and February. In spring, summer and autumn, there were positive ASTD values near Taiwan and negative values over most of the SCS. In June, the difference of ASTD between the two sea areas minimized. In August, the ASTD near Taiwan was positive and a negative peak over most of the SCS.

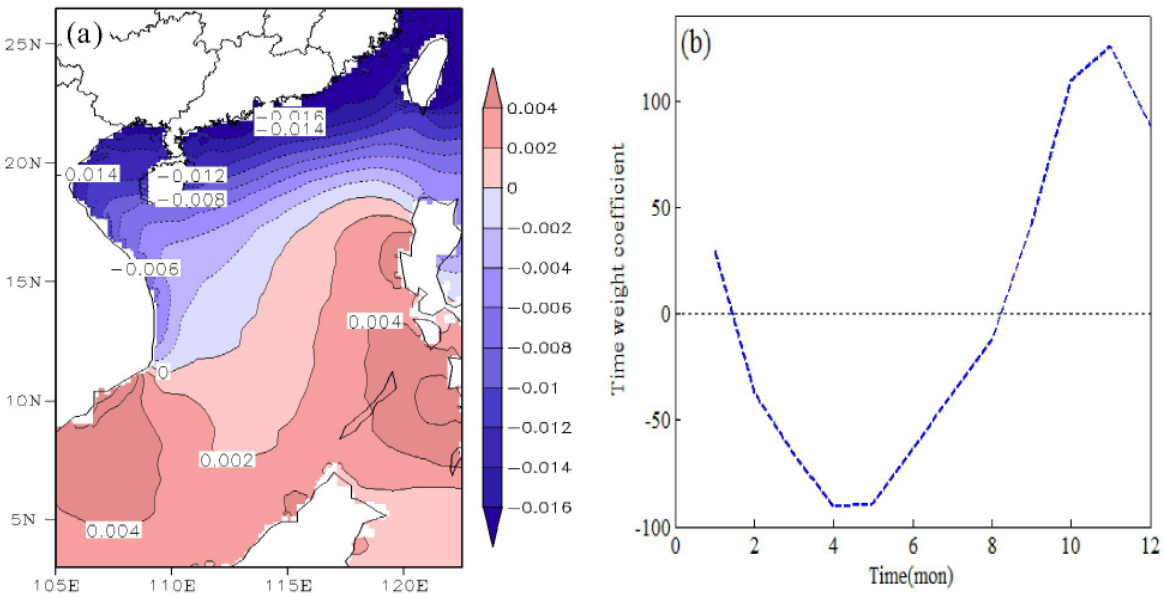

Figure 6. First mode of average climate state of ASTD over the SCS. a. eigenvectors; b. time weight coefficient.

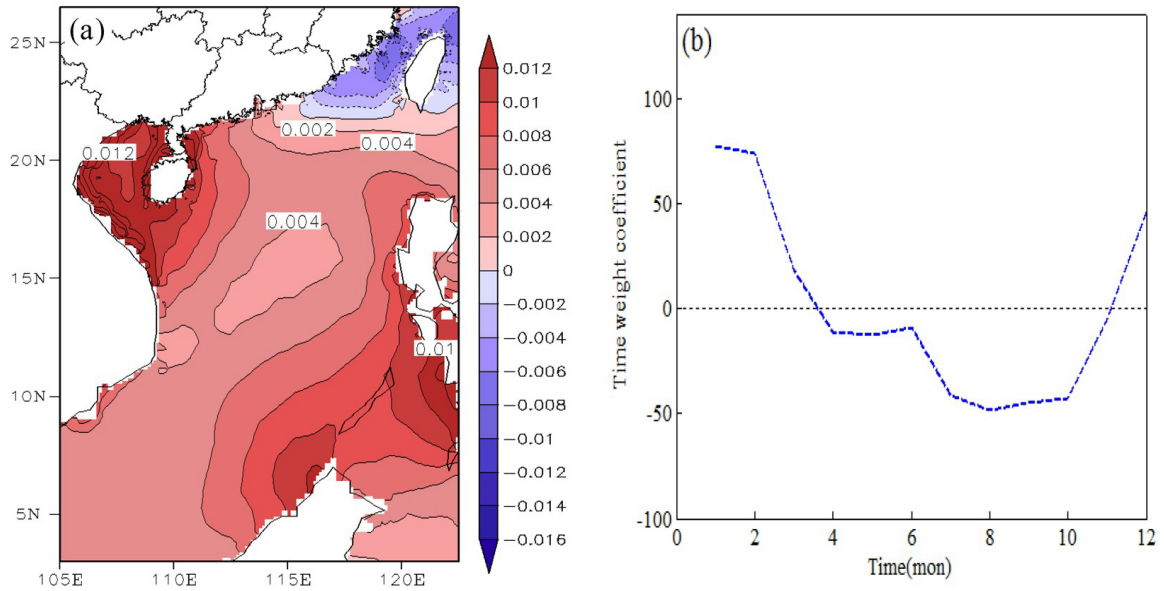

Figure 7. Second mode of average climate state of ASTD over SCS. a. eigenvectors; b. time weight coefficient

4.2 *Interannual variations*

Based on the ERA-Interim data, monthly average ASTD in the SCS from June to August for the past 35 years was converted to anomalies. EOF decomposition was used to determine spatiotemporal distributions of summer ASTD variation across the SCS. The first three rate of variance contributions of eigenvectors were 44.49%, 16.60% and 10.31%, making up a total of 71.40% of the information on ASTD summer variation over the SCS. Combining the first mode of the eigenvectors with the time weight coefficient (Fig.8) showed a seesaw-type ASTD distribution between Beibu Bay and most of the SCS in summer. Interannual variations of ASTD strongly decreased over the SCS. In summer 1998, the ASTD in the SCS was maximum. In the summers of 1995 and 2010, the ASTD was large, being positive in Beibu Bay and negative across most of the SCS.

Using the ERA-Interim data, the monthly average ASTD over the SCS from September to December for the past 35 years was converted to anomalies. Additionally, we used EOF decomposition to determine spatiotemporal distributions of autumn ASTD variation. The first three rate of variance contributions of eigenvectors were 41.08%, 17.30%, and 12.58%, constituting a total of 70.96% of information on autumn ASTD variation over the SCS. Combining the first

mode of the eigenvectors with the time weight coefficient (Fig.9), interannual ASTD variations in autumn are obviously decreasing over the SCS. In autumn 1998, ASTD of the SCS maximized, with the second maximum during autumn 2010. There were positive values of ASTD in the northern SCS and negative ones in the south. Large values of ASTD formed a closed field. The dominant large value area was in the southern SCS, whose center nearly covered all of the Nansha Islands area. Another center of large values was southeast of Taiwan Island.

In El Niño years, seasonal variations of SST showed anomalies, which led to abnormal ASTD seasonal variations. As known, there were ENSO events during the periods 1991–1994, 1997–1998, and 2009–2010. Analyzing the first mode of ASTD in the SCS area for spring and autumn indicate that the abnormal ASTD peak may be related to ENSO events.

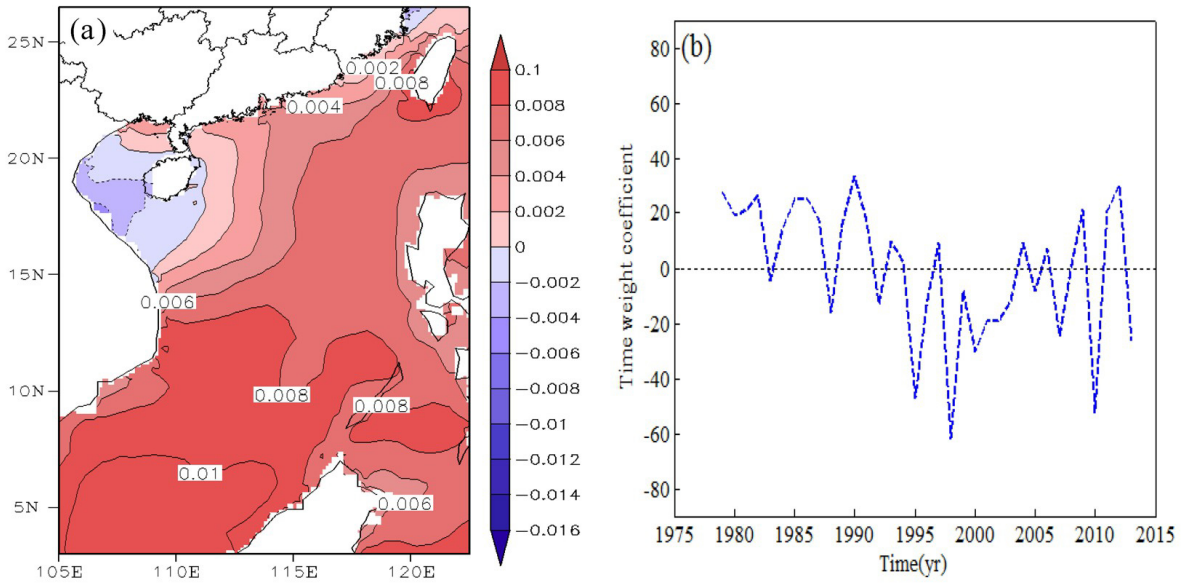

Figure 8. First mode of ASTD over SCS in summer. a. eigenvectors; b. time weight coefficient.

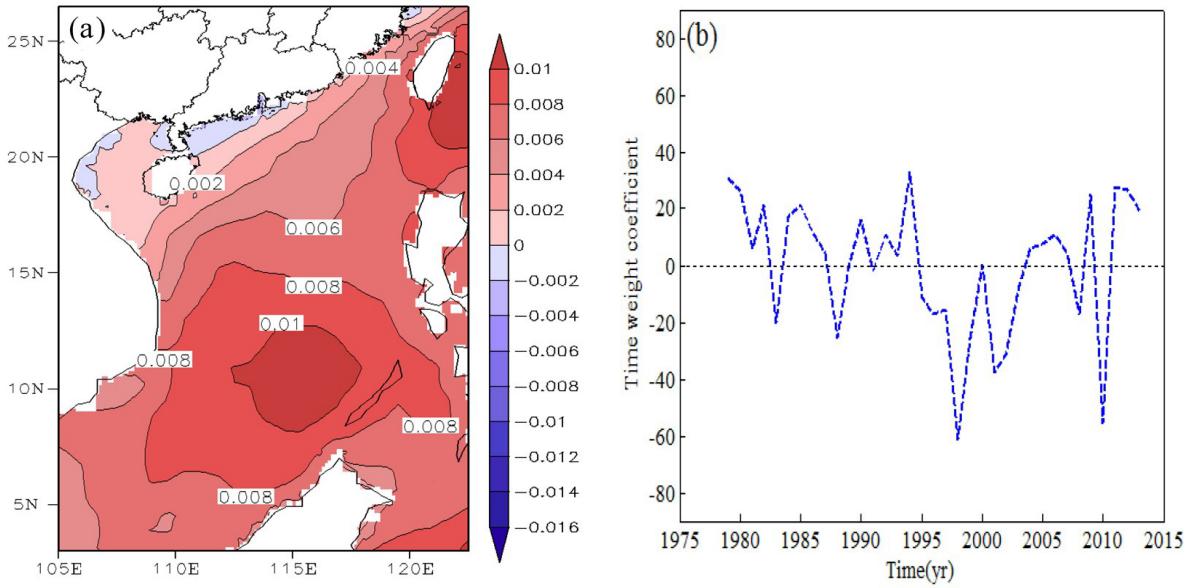

Figure 9. First mode of ASTD over SCS in autumn. a. eigenvectors; b. time weight coefficient

5 ASTD AND NINO3.4 INDEX

5.1 *Wavelet analysis of first mode of ASTD*

To address the relationship between ASTD in the SCS and the ENSO cycle, time series of the first ASTD mode was analyzed using Morlet wavelet transformation in different seasons (Fig.10). This shows strong quasi-2a, quasi-3-5a, and quasi-11a periods in spring (Fig.10a), a strong quasi-3a period in summer (Fig.10b), strong quasi-2-3a period in autumn (Fig.10c), and strong quasi-3a and quasi-11a periods in winter (Fig.10d). Thus, the ASTD across the SCS has a strong quasi-3a oscillation period in spring, summer, autumn and winter. It also has a strong quasi-5a period in spring. In contrast with the 2-7a periods of the ENSO cycle, its main period of 3-5a is basically consistent with the results[10,11]. In addition, the ASTD across the SCS has a quasi-11a period in spring and winter.

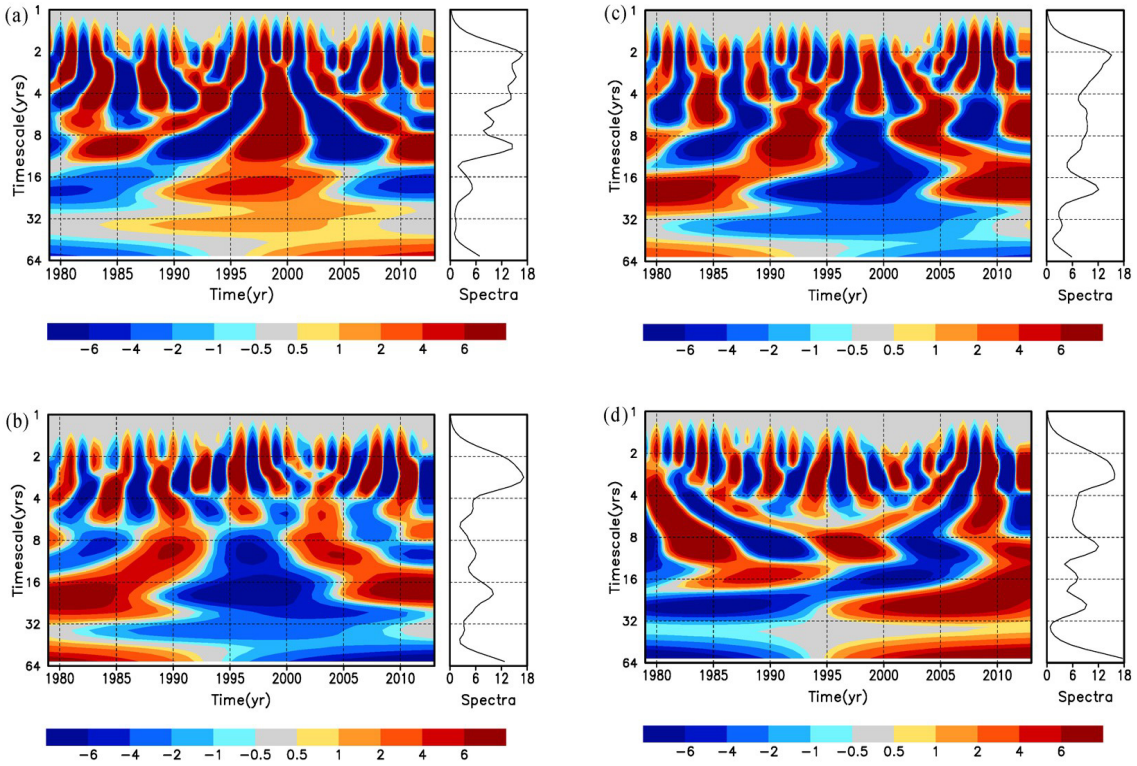

Figure 10. Wavelet analysis of ASTD PC1 over SCS in four seasons. a. spring; b. summer; c. autumn; d. winter.

5.2 *Time series of ASTD and Niño3.4 index*

The EOF time series of the first ASTD mode over the SCS in spring, summer, autumn, and winter were determined, which gave correlations with the Niño 3.4 index series (Fig.11). The correlation coefficient is shown in Table 1.

Table 1. Correlation coefficient of ASTD time series for the SCS in each season and Niño3.4 index.

season	spring	summer	autumn	winter
correlation coefficient	−0.69	0.36	0.36	−0.46

Table 1 shows that the ASTD was strongly negatively correlated with the Niño 3.4 index in winter and spring, and weakly positively correlated in summer and autumn. As is shown in Fig. 11, absolute values of the Niño3.4 index are larger in every season of 1987, 1998, 1999 and 2010. However, from our analyses above, we know that ASTD maxima were in 1998 and 2010. This suggests that the ASTD anomalies are related to the ENSO cycle. However, details of this relationship remains to be further investigated.

6 CONCLUSIONS

By comparing ASTD fields with two different datasets of the SCS and addressing intra-annual and interannual spatiotemporal ASTD characteristics there, the following conclusions were obtained.

(1) Both ICOADS and ERA-Interim data can be used to fully describe the characteristics of ASTD over the SCS. Values of ASTD based on the ERA-Interim data are smaller than those based on ICOADS data in the same region. However, inshore ASTD characteristics from the ICOADS data are more pronounced than those from the ERA-Interim data.

(2) There is a seesaw-type ASTD distribution between the southern and northern SCS. In autumn and

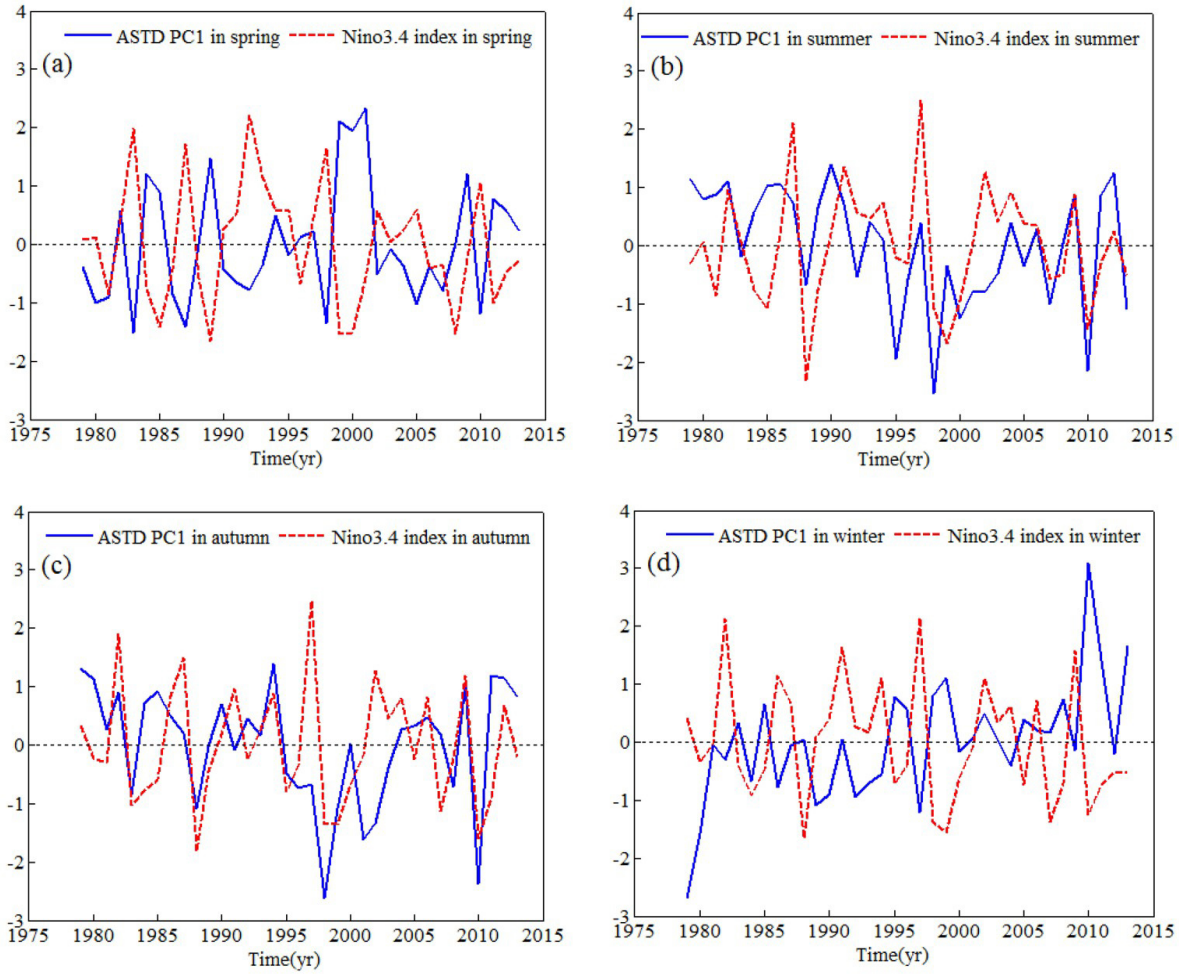

Figure 11. Correlation curve of ASTD PC1 over SCS in four seasons a. spring; b. summer; c. autumn; d. winter

winter, ASTD values are positive in the south and negative in the north, with November maxima. In spring and summer, there are positive ASTD values in the north and negative ones in the south, with maxima in April and May.

(3) Interannual variations of ASTD in summer or autumn are decreasing. There is a seesaw-type ASTD distribution between Beibu Bay and most of the SCS in summer. There are two closed centers of large values in the autumn ASTD field. The center of large values is in the Nansha Islands area in that season.

(4) The ASTD over the SCS has a strong quasi-3a oscillation period in all four seasons, a strong quasi-5a period in spring, and a quasi-11a period in spring and winter.

(5) The ASTD is weakly positively correlated with the Niño3.4 index in summer and autumn but strongly negatively correlated with that index in winter and spring.

REFERENCES:

[1] WANG Bin-hua. Sea Fog [M]. China Ocean Press, Beijing, 1983: 352.

[2] ZHANG Su-ping, REN Zhao-peng. The influence of the thermal effect of underlaying surface on the spring sea over the Yellow Sea: Observations and numerical simulations [J]. Acta Meteor Sinica, 2010, 68(4): 439-449.

[3] HUANG Hui-jun. Observation and analysis of the structure of the sea fog and its boundary layer in the coastal area of Southern China [D]. Nanjing University, Nanjing, 2013.

[4] YANG Cai-fu, LIU Ai-guo. The statistical analysis of the daily change in the South China Sea influenced by cold air [J]. Marine Forecasts, 2001, 18(1): 59-64.

[5] LIN Ai-lan, LIANG Jian-yin, GU De-jun, et al. On the relationship between convection intensity of South China Sea summer monsoon and air-sea temperature difference in the tropical oceans [J]. Acta Oceanol Sinica, 2004, 23(2): 267-278.

[6] JI Wen-jun, ZHANG Shu-wen, ZHAO Hui, et al. Impact of the sea surface coefficient CD to the air-sea temperature difference [J]. Marine Forecasts, 2013, 30(5): 64-68.

[7] XUE De-qiang. El Niño and the Qingdao Binhai air sea temperature difference [J]. Marine Sci Bull, 1994, 13(2): 90-92.

[8] WANG Shao-wen, XUE De-qiang, ZHAO Xu-kong. The series of Variations in the Difference Between the Coastal SST and Air Temperature in Qingdao and Yantai [J]. J Oceanogr Huanghai & Bohai Seas. 1994, 12(2): 57-60.

[9] LI Xiao-ting, ZHENG Pei-nan, WANG Jian-feng, et al. Introduction of the ocean data in common use [J]. Marine Forecasts, 2010, 27(5): 81-89.
[10] YAN Hong, SUN Li-guang, LIU Xiao-dong, et al. Relationship between ENSO events and regional climate anomalies around the Xisha Islands during the last 50 years [J]. J Trop Oceanogr, 2010, 29(5): 29-35.
[11] REN Rong-cai. Study of the lag-coupling between the 3-5 year timescale ENSO events and the stratospheric circulation in the past 60 years and its mechanism [J]. Acta Meteor Sinica, 2012, 70(3): 520-535.

Citation: XU Feng, XIA Tian-zhu, WANG Hui et al. Comparative analysis of various data of air-sea temperature difference and its variation across South China Sea in the past 35 years [J]. J Trop Meteor, 2017, 23(3): 292-301.